



ARTICLE

<https://doi.org/10.1038/s41467-019-11149-1>

OPEN

Evolution of metazoan oxygen-sensing involved a conserved divergence of VHL affinity for HIF1 α and HIF2 α

Daniel Tarade ¹, Jeffrey E. Lee¹ & Michael Ohh ^{1,2}

Duplication of ancestral hypoxia-inducible factor (HIF) α coincided with the evolution of vertebrate species. Paralogs HIF1 α and HIF2 α are the most well-known factors for modulating the cellular transcriptional profile following hypoxia. However, how the processes of natural selection acted upon the coding region of these two genes to optimize the cellular response to hypoxia during evolution remains unclear. A key negative regulator of HIF α is von Hippel-Lindau (VHL) tumour suppressor protein. Here we show that evolutionarily-relevant substitutions can modulate a secondary contact between HIF1 α Met561 and VHL Phe91. Notably, HIF1 α binds more tightly than HIF2 α to VHL due to a conserved Met to Thr substitution observed in the vertebrate lineage. Similarly, substitution of VHL Phe91 with Tyr, as seen in invertebrate species, decreases VHL affinity for both HIF1 α and HIF2 α . We propose that vertebrate evolution involved a more complex hypoxia response with fine-tuned divergence of VHL affinity for HIF1 α and HIF2 α .

¹Department of Laboratory Medicine & Pathobiology, University of Toronto, 1 King's College Circle, Toronto, ON M5S 1A8, Canada. ²Department of Biochemistry, University of Toronto, 661 University Avenue, Toronto, ON M5G 1M1, Canada. Correspondence and requests for materials should be addressed to M.O. (email: michael.ohh@utoronto.ca)

Metazoan oxygen-sensing requires hypoxia-inducible factor (HIF) α proteins¹. These oxygen-labile transcription factors are present at low to non-detectable levels under normoxic conditions in metazoan cells but are stabilized at the protein level under hypoxic conditions. In a series of experiments, it was shown that HIF α protein is rapidly hydroxylated on conserved proline residues found within its oxygen-dependent degradation (ODD) domain by prolyl hydroxylase domain containing enzymes (PHDs)². The hydroxylation of the proline residues allows recognition of HIF α by von Hippel-Lindau (VHL) protein, which serves as the substrate-conferring component of an E3 ubiquitin ligase complex^{3–5}. The hydroxylation of HIF α via PHDs requires molecular oxygen as a co-substrate. Thus, hydroxylation of HIF α results in oxygen-dependent, ubiquitin-mediated, proteasomal degradation. Under hypoxic conditions, HIF α escapes both hydroxylation via PHDs and recognition via VHL allowing its dimerization with the constitutively expressed HIF β protein. This dimerization results in the formation of a functional transcription factor that upregulates expression of angiogenic factors, glycolytic enzymes, and signalers of erythropoiesis, among other genes.

All eumetazoans, except ctenophera, express, at minimum, a single HIF α , PHD, and VHL gene⁶. The simplest metazoan to express the full complement of PHD, VHL, and HIF α genes is *T. adhaerens*⁷. PHD cloned from *T. adhaerens* can function to regulate HIF α when expressed in human cells, suggesting remarkable conservation of this pathway during metazoan evolution⁷. Crystallization of *T. adhaerens* PHD bound to its corresponding HIF α peptide reveals significant structural conservation with human PHD2 bound to human HIF α peptides⁸. However, despite conservation of the core proteins critical for oxygen-sensing throughout the majority of animal evolution, duplication of the genes encoding these proteins is observed. All examined invertebrate species possess only one HIF α gene and at most two PHD genes⁷. Interestingly, HIF α is observed to have undergone multiple duplication events coinciding with the evolution of vertebrate species⁷.

In humans, there are three HIF α proteins, HIF1 α , HIF2 α , and HIF3 α , among which the former two are best characterized. There are considerable similarities between HIF1 α and HIF2 α proteins, which have 48% primary amino acid sequence identity⁹. The primary hydroxylation sites are P564 and P531 in HIF1 α and HIF2 α (C-terminal oxygen-dependent degradation domain or CODD sites), respectively, while the corresponding secondary hydroxylation sites are P402 and P405 (N-terminal ODD or NODD sites). Structural data obtained from co-crystallization of HIF1 α and HIF2 α CODD peptides with the VHL regulatory complex reveal a similar binding motif for the two protein homologs^{10–12}. There is also high structural conservation between HIF1 α and HIF2 α basic helix loop helix (bHLH) and PER-ARNT-SIM (PAS) domains, which are responsible for DNA binding and dimerization with HIF β , respectively¹³.

Although HIF1 α and HIF2 α are regulated by PHDs and VHL in a similar manner, several differences exist between the two proteins. Firstly, HIF1 α and HIF2 α are not redundant during mouse embryogenesis. HIF1 α ^{-/-} mice are embryonic lethal (E11) as a result of defects in neural tube and cardiovascular development^{14,15}. HIF2 α ^{-/-} mice also die during embryogenesis due to defects in catecholamine synthesis or vascular disorganization^{16,17}. However, the penetrance and timing of embryonic lethality appears to depend on the genetic background^{16,17}. Furthermore, despite the fact that HIF1 α and HIF2 α both recognize the canonical hypoxia-responsive element (HRE; 5'-RCGTG-3') and regulate a common set of genes, each also regulates a set of unique transcriptional targets^{18,19}. For example, regulation of genes encoding glycolytic enzymes is

mostly carried out by HIF1 α whereas HIF2 α is the near-exclusive binder of HREs associated with members of the Oct4 family¹⁸. Additionally, although HIF1 α and HIF2 α both appear to contribute to the pathogenesis of clear cell renal cell carcinoma (ccRCC) in the context of *VHL* loss, they appear to play different roles. A series of experiments with transgenic mice show that HIF1 α but not HIF2 α activation results in metabolic reprogramming and promotion of the clear cell phenotype that is important for tumour initiation^{20–22}. Conversely, HIF2 α has been shown to be necessary for the growth of xenograft tumours^{23,24}. Lastly, HIF1 α responds acutely to hypoxia while HIF2 α is largely a chronic responder to hypoxia due in part to its less efficient degradation²⁵. Despite well-documented differences between HIF1 α and HIF2 α , how natural selection acted upon the coding region of these two genes during the evolution of vertebrate species has only been studied using computational methods²⁶. We sought to identify substitutions that uniquely impacted one of the HIF α paralogs and to evaluate the potential impact on protein function, which may have facilitated increased complexity of the oxygen-sensing pathway.

Here, we show that HIF1 α binds more tightly to VHL than HIF2 α due to a conserved substitution in the vertebrate lineage affecting an amino acid proximal to the primary hydroxylation site. HIF1 α Met561 but not HIF2 α Thr528 stabilizes the interaction with VHL by favourably packing against VHL Phe91. Similarly, VHL F91Y substitution, which mimics a common invertebrate substitution, results in decreased VHL affinity for both HIF1 α and HIF2 α . Thus, we propose that following the emergence of the vertebrate clade, these conserved substitutions resulted in a functional divergence in VHL-mediated negative regulation of HIF1 α and HIF2 α , allowing more specialized hypoxic signalling.

Results

HIF1 α has a higher affinity for VHL than HIF2 α . The relative affinities of VHL for the two major paralogs of HIF α have not been previously reported. As it has been suggested that HIF2 α is less efficiently degraded when compared to HIF1 α , we hypothesized that HIF1 α may interact more strongly with VHL. In a pulldown assay, we observed that hydroxylated HIF1 α peptide (556–573) pulls down more in vitro transcribed and translated (IVTT) HA-VHL than HIF2 α peptide (523–541; Fig. 1a). Furthermore, acetylated HIF1 α peptide competes more effectively for HA-VHL than HIF2 α peptide (Fig. 1b). These results suggest that HIF1 α binds more tightly to VHL than HIF2 α .

HIF1 α Met_{n-3} stabilizes interaction with VHL. We have previously noted that in the immediate vicinity of the primary hydroxylation sites there are several residues that are not conserved between HIF1 α and HIF2 α ¹², including the amino acid three residues N-terminal of the primary hydroxylation site, HIF1 α Met_{n-3} and HIF2 α Thr_{n-3} (n denotes the primary hydroxylation site; Fig. 2a). We hypothesized that this difference in affinity for VHL might be mediated by the divergent biochemical properties of HIF1 α Met_{n-3} and HIF2 α Thr_{n-3}. To test this hypothesis, we designed a HIF1 α hybrid screen whereby residues that are not conserved between HIF1 α and HIF2 α are substituted to the corresponding HIF2 α residue (Fig. 2a). Indeed, HIF1 α M561T pulled down similar levels of HA-VHL when compared to HIF2 α wild-type (WT), while other substitutions designed to mimic HIF2 α , including insertion of Gly_{n+6}, had no effect on affinity for VHL (Fig. 2b). Substitution of HIF1 α Met561 with alanine was also found to reduce affinity toward VHL to levels similar to HIF2 α WT (Supplementary Fig. 1a). Importantly, the reciprocal HIF2 α T528M substitution resulted in increased

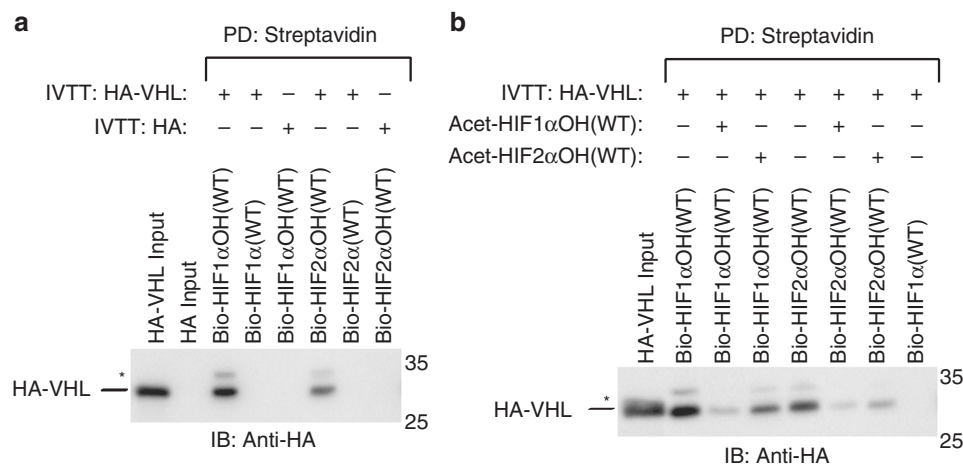


Fig. 1 VHL has a higher affinity for HIF1 α than HIF2 α . **a, b** Biotinylated HIF α OH peptides were immobilized on streptavidin- agarose beads and incubated with in vitro transcribed and translated (IVTT) HA-VHL. Where indicated, acetylated HIF α OH peptides were included during the pull down. Streptavidin beads were pulled down (PD) and levels of HA- VHL were visualized via immunoblotting (IB). Molecular weight markers (kDa) are labeled for western blots

affinity for VHL while deletion of G537 resulted only in a minor decrease in affinity for VHL (Supplementary Fig. 1b). To further evaluate the effect of Met/Thr_{n-3} on HIF α /VHL complex stability, we performed biolayer interferometry (BLI), where the rate at which purified VHL-elongin B-elongin C (VBC) complex associates and dissociates to and from immobilized HIF α peptide can be measured (Supplementary Fig. 2a). We found that Met_{n-3}, as found in HIF1 α WT, is associated with a dissociation rate that is 1.7 to 1.8 times slower than peptides containing Thr_{n-3} (HIF2 α WT; Fig. 2c, d and see BLI sensorgrams in Supplementary Fig. 2a). The kinetic values were validated using surface plasmon resonance (SPR; Supplementary Fig. 2b). We found that HIF1 α WT had a dissociation rate ($0.024 \pm 0.0007 \text{ s}^{-1}$) that was slower than both HIF2 α WT ($0.067 \pm 0.004 \text{ s}^{-1}$) and HIF1 α M561T ($0.076 \pm 0.01 \text{ s}^{-1}$; Supplementary Fig. 2c). Next, immunoprecipitation of IVTT 3xFLAG-HIF1 α (387–581) revealed that the M561T substitution resulted in decreased affinity of HIF1 α ODD protein for VHL while the T528M substitution increased the affinity of 3xFLAG-HIF2 α (390–554) ODD protein for VHL (Fig. 2e, Supplementary Fig. 1c). Thus, we find that non-conserved residues in the proximity of the primary hydroxylation site of HIF1 α and HIF2 α dictate different binding affinity to VHL.

HIF1 α Met_{n-3} is conserved in vertebrate species. Having shown that HIF α Met_{n-3} increases affinity for VHL, we next asked whether this residue is conserved in metazoan species. First, a maximum-likelihood phylogenetic tree was constructed using the cDNA sequences corresponding to the ODD domain of HIF1 α (Fig. 3a). The maximum-likelihood method attempts to minimize the number of evolutionary events required to explain the sequence data while also allowing for variable rates of evolution across sites and branches. Generally, known relationships between major clades of metazoan species are recovered in our experimental phylogenetic tree. Subsequently, we estimated synonymous (dS) and non-synonymous (dN) mutation rates for codons in the HIF1 α ODD domain (Fig. 3b). Interestingly, dN/dS ratios were lower in the vertebrate lineage than in the invertebrate lineage for most codons but the trend was most apparent for codons corresponding to the NODD and CODD regions (Fig. 3b). This suggests that the ODD domain in vertebrate species is under more stringent negative selection. Among the codons that had a lower dN/dS ratio in vertebrate species is Met_{n-3}. When considering the alignment of amino acid sequences

from 29 vertebrate and 22 invertebrate species, we observed that Met_{n-3} is conserved in vertebrate species but variable in invertebrate species (Fig. 3c, Supplementary Fig. 3). Like HIF1 α Met_{n-3}, HIF2 α Thr_{n-3} is conserved in vertebrate species. The one notable exception is the lamprey (*P. marinus*), where both HIF1 α and HIF2 α sequences contain Met_{n-3} (Supplementary Fig. 3). Thus, not only are HIF1 α Met_{n-3} and HIF2 α Thr_{n-3} associated with distinct affinities for VHL, these residues are incredibly conserved in species expressing both HIF1 α and HIF2 α , suggesting that the specialization of VHL affinity is of importance.

Methionine oxidation decreases HIF1 α affinity for VHL. Co-crystallization of HIF1 α OH peptide with VBC complex has shown that HIF1 α Met561 packs against VHL Phe91^{10,11}. We recently co-crystallized HIF2 α OH peptide with VBC complex and showed that substitution of Met_{n-3} with Thr does not result in local conformational changes, with HIF2 α Thr528 remaining in proximity to VHL Phe91¹². It has been previously noted that the methionine-aromatic interaction is enriched within known protein structures and, according to quantum mechanical calculations, the interaction is predicted to contribute 1.0–1.5 kcal/mol of additional stability when compared to the interaction between an aromatic residue and a bulky nonpolar residue²⁷. The average distance between the sulfur (Met) and aromatic ring center is 5 Å with a preferential orientation of 30–60°²⁷. When analyzing two available HIF1 α -VBC structures, the distance between the sulfur atom of HIF1 α Met561 and the ring center of VHL Phe91 ranges between 4.58 Å (1LQB) and 4.80 Å (1LM8; Fig. 4a). The angle between the sulfur atom of HIF1 α Met561 and the vector normal to the aromatic plane ranges from 41.3° to 42.9° (Fig. 4a). Concordantly, in silico analysis of the binding interface between VHL and HIF1 α (1LM8) or VHL and HIF2 α (6BVB) suggests that HIF1 α Met561 contributes greater stability to the HIF/VHL complex than HIF2 α Thr528 (1.41 kcal/mol versus 0.75 kcal/mol). Further, VHL Phe91 is more buried when bound by HIF1 α peptide (41.2% buried surface area/accessible surface area) than by HIF2 α peptide (32.7%). Thus, there appears to be a structural basis for the preferential binding of Met_{n-3} containing peptides to VHL when compared to peptides where Met_{n-3} is instead substituted with Thr or Ala.

Oxidation of methionine to methionine sulfoxide (MetO) has been implicated in cellular signalling. However, there is an ongoing discussion about whether oxidation of Met increases or

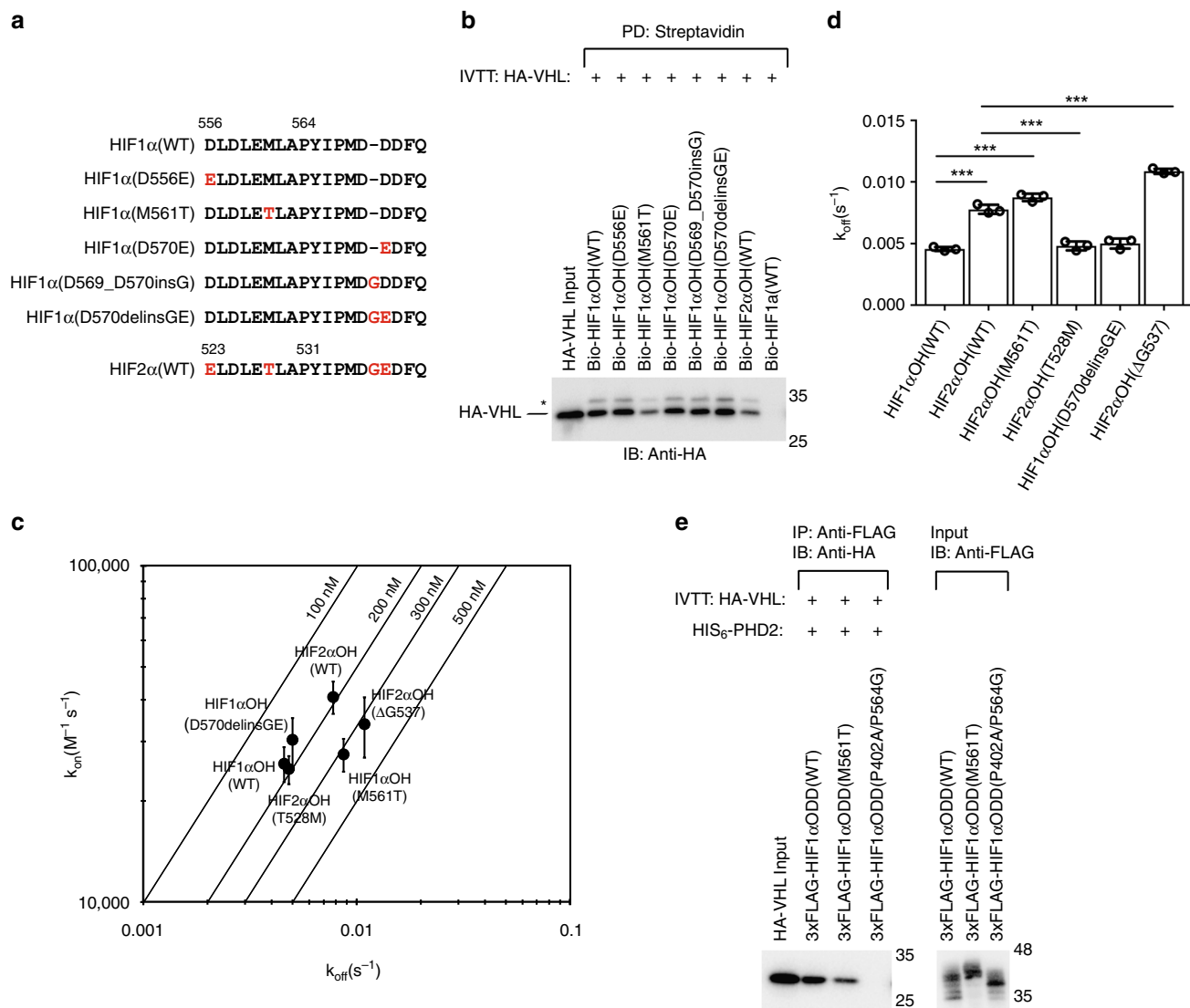


Fig. 2 HIF1 α Met_{n-3} stabilizes interaction with VHL. **a** Peptide sequences used in subsequent experiments are listed. Peptides are N-terminal biotinylated. Numbering is provided for the N-terminal amino acid residue and the proline hydroxylation site. **b** Biotinylated HIF α OH peptides were immobilized on streptavidin- agarose beads and incubated with in vitro transcribed and translated (IVTT) HA-VHL. Streptavidin beads were pulled down (PD) and levels of HA-VHL were visualized via immunoblotting (IB). **c, d** Biolayer interferometry kinetic analysis of VHL-elongin B-elongin C (VBC) complex binding to immobilized HIF α peptides. Biotinylated peptides were immobilized on streptavidin- coated biosensors and binding to VBC complex was monitored. The data was analyzed assuming a 1:1 binding model via the BLItz Pro software. **c** Rate plane with Isoaffinity Diagonals (RaPID) plot highlighting the kinetic parameters of VBC complex binding to HIF α peptides. Values represent mean of three experiments conducted with independently purified protein \pm s.e.m. **d** The dissociation constants associated with VBC binding to HIF α peptides are shown on a linear scale. Statistical significance was assessed using a one-way ANOVA with Tukey's post hoc test. Values represent mean of three experiments conducted with independently purified protein \pm s.d. *** $p < 0.005$. **e** 3xFLAG-HIF1 α oxygen-dependent degradation (ODD) domains were IVTT and incubated with purified HIS₆-PHD2 (181-426). Following hydroxylation (one hour), 3xFLAG-HIF1 α ODD domain was immobilized on protein A beads coated with anti-FLAG antibody and incubated with IVTT HA-VHL. 3xFLAG-HIF1 α ODD domain was immunoprecipitated (IP) and levels of HA-tagged VHL were visualized via immunoblotting (IB). Molecular weight markers (kDa) are labeled for western blots

decreases its affinity for aromatic residues. When the Met-aromatic interaction is simulated in the gaseous phase, it is evident that methionine oxidation increases the affinity of methionine for aromatic compounds, such as benzene^{28,29}. However, the stability of the MetO-aromatic interaction is diminished when simulated in an aqueous environment. In an article by Lewis et al., the MetO-aromatic interaction was reported to still be more favourable than Met-aromatic in an aqueous environment yet a report by Orabi et al., instead suggested that Met interacts more strongly than MetO with aromatic compounds in an aqueous environment due to a

solvation effect driven by increased hydrophilicity^{28,29}. As the tested HIF α peptides are poorly soluble, they are reconstituted in DMSO for most of the reported experiments. To ensure that the increased binding of HIF1 α to VHL is not driven by potential artefactual oxidation of HIF1 α Met561 to MetO561 in DMSO, we tested peptides dissolved in an aqueous buffer. HIF1 α OH peptide solubilized in DMSO or an aqueous buffer pulled down similarly more VHL than the corresponding HIF2 α OH peptides (Fig. 4b). However, synthetic oxidation of HIF1 α Met561 but not Met568 resulted in decreased affinity for VHL (Fig. 4c). Complete oxidation of HIF1 α Met561 to methionine sulfone (MetO₂)

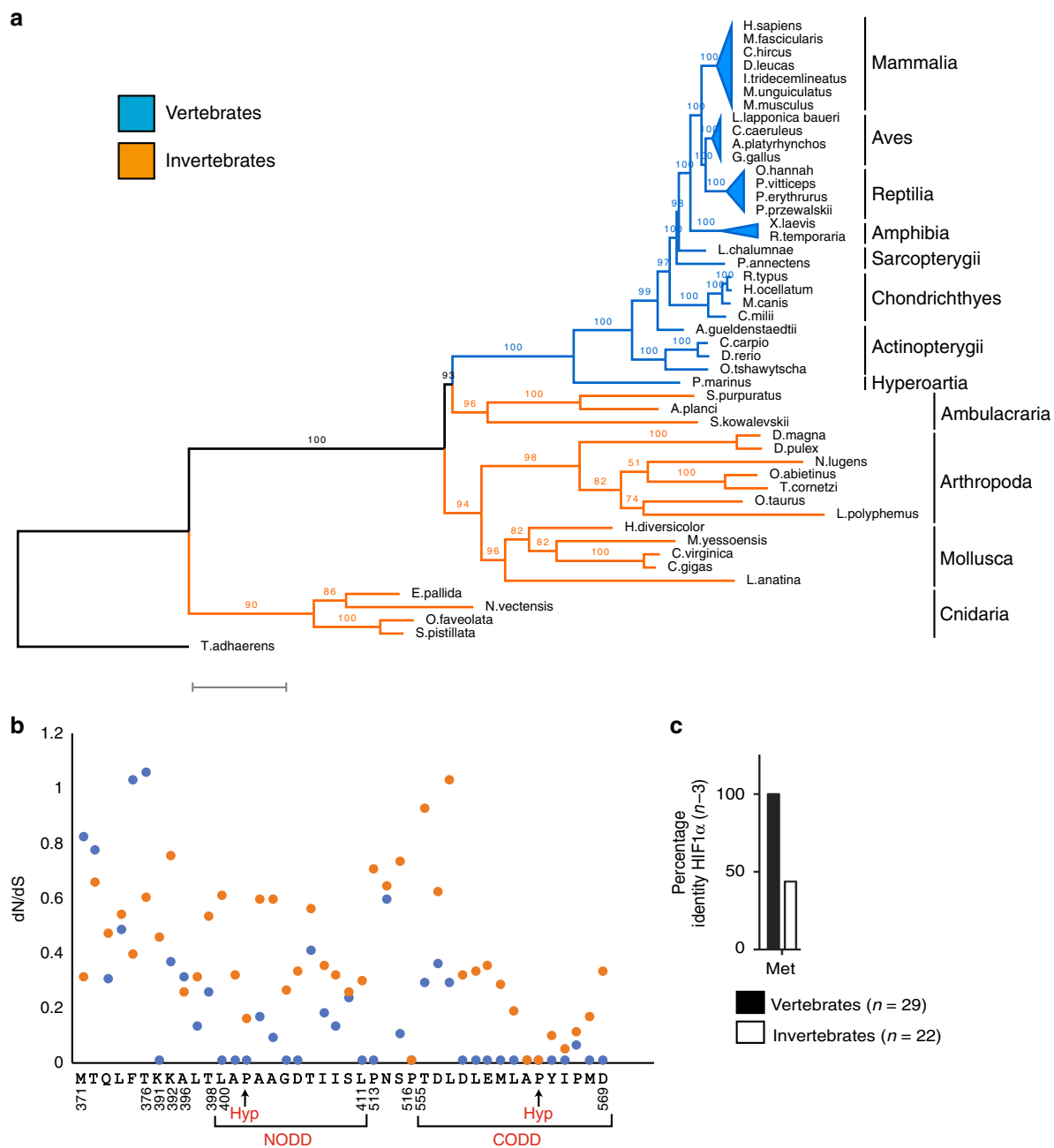


Fig. 3 HIF α Met $_{n-3}$ is conserved in the vertebrate lineage. **a, b** Blue = vertebrate; orange = invertebrate. Full-length HIF1 α cDNA sequences were aligned. The region corresponding to the oxygen-dependent degradation (ODD) domain was re-aligned and the top 21 alignments were concatenated. **a** A maximum-likelihood phylogenetic tree was constructed. Branch values indicate bootstrap support (100 bootstraps). Scale bar, 0.7 substitutions per site. **b** Non-synonymous (dN) and synonymous (dS) substitution rates were estimated for codons that aligned without gaps using the HyPhy software accessed via Mega7. The amino acid residue and numbering correspond to human HIF1 α . **c** Annotated HIF1 α amino acid sequences (full-length) were identified through use of BLASTP. Sequences were aligned using the MAFFT algorithm via the GUIDANCE2 webserver. The frequency of the amino acid three residues N-terminal of the primary hydroxylation site is indicated for vertebrate and invertebrate species

resulted in a further decrease in VHL affinity (Fig. 4c). Although oxidation of Met561 and Met568 resulted in a significant increase in the dissociation rate of VHL from HIF1 α OH peptide, only oxidation of Met561 resulted in an increase in dissociation rate comparable to the M561T substitution (Fig. 4d, e). Substitution of HIF1 α Met561 with norleucine did not affect the affinity of HIF1 α OH peptide for VHL (Fig. 4c). These results suggest that the sulfur atom of methionine is not necessary for the increased stability of the HIF1 α OH-VHL complex and that oxidation of HIF1 α Met561 results in a decreased affinity for VHL, consistent with the model proposed by Orabi et al.

Ancestral VHL protein binds poorly to HIF α . Differential affinity of Met and Thr residues for aromatic residues provides a structural and biochemical rationale for differential binding of HIF1 α and HIF2 α to VHL. As we observed that HIF1 α Met $_{n-3}$ is conserved in vertebrates but variable among invertebrate species, we asked whether VHL Phe91 followed a similar pattern of evolution. As the numbering of amino acids differs among species, we will refer to residues that align with VHL Phe91 as VHL X $_{n+3}$, where n refers to an invariant tryptophan residue (VHL Trp88 in humans) that forms part of the hydroxylproline binding pocket. Strikingly, we found that VHL Phe $_{n+3}$ is conserved in

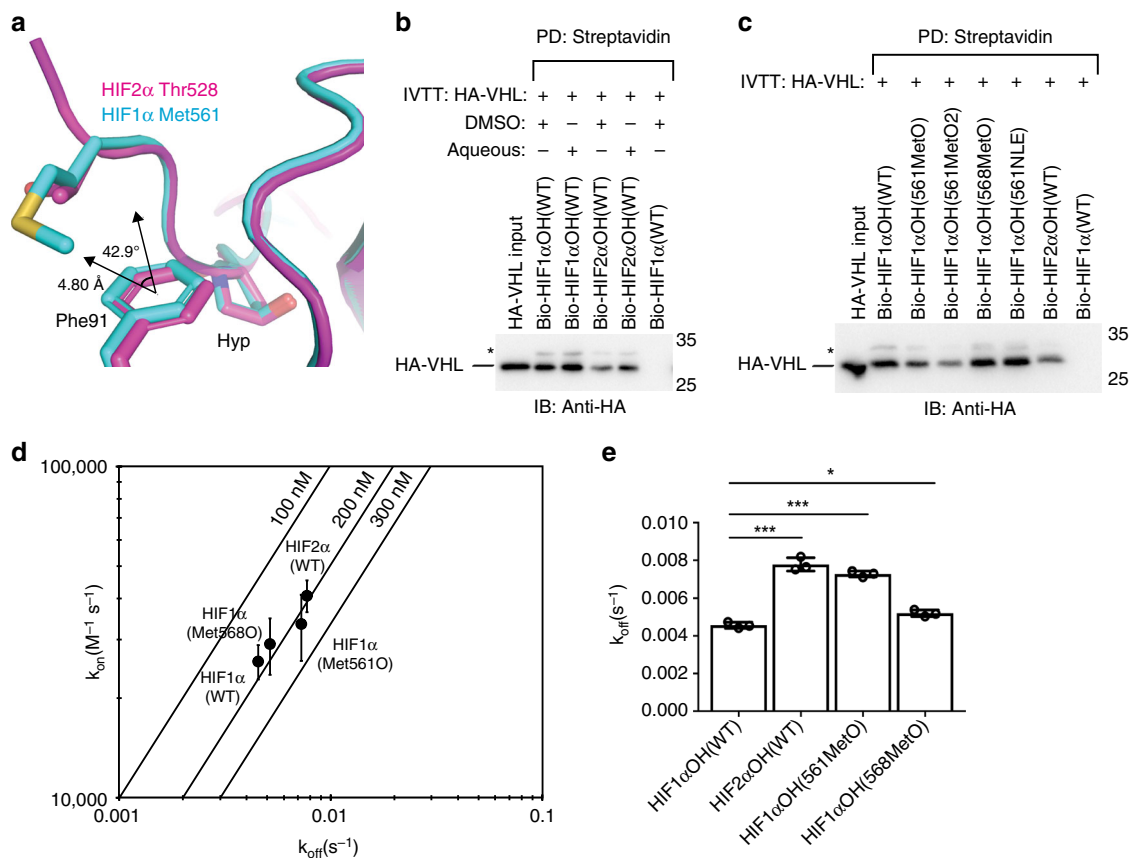
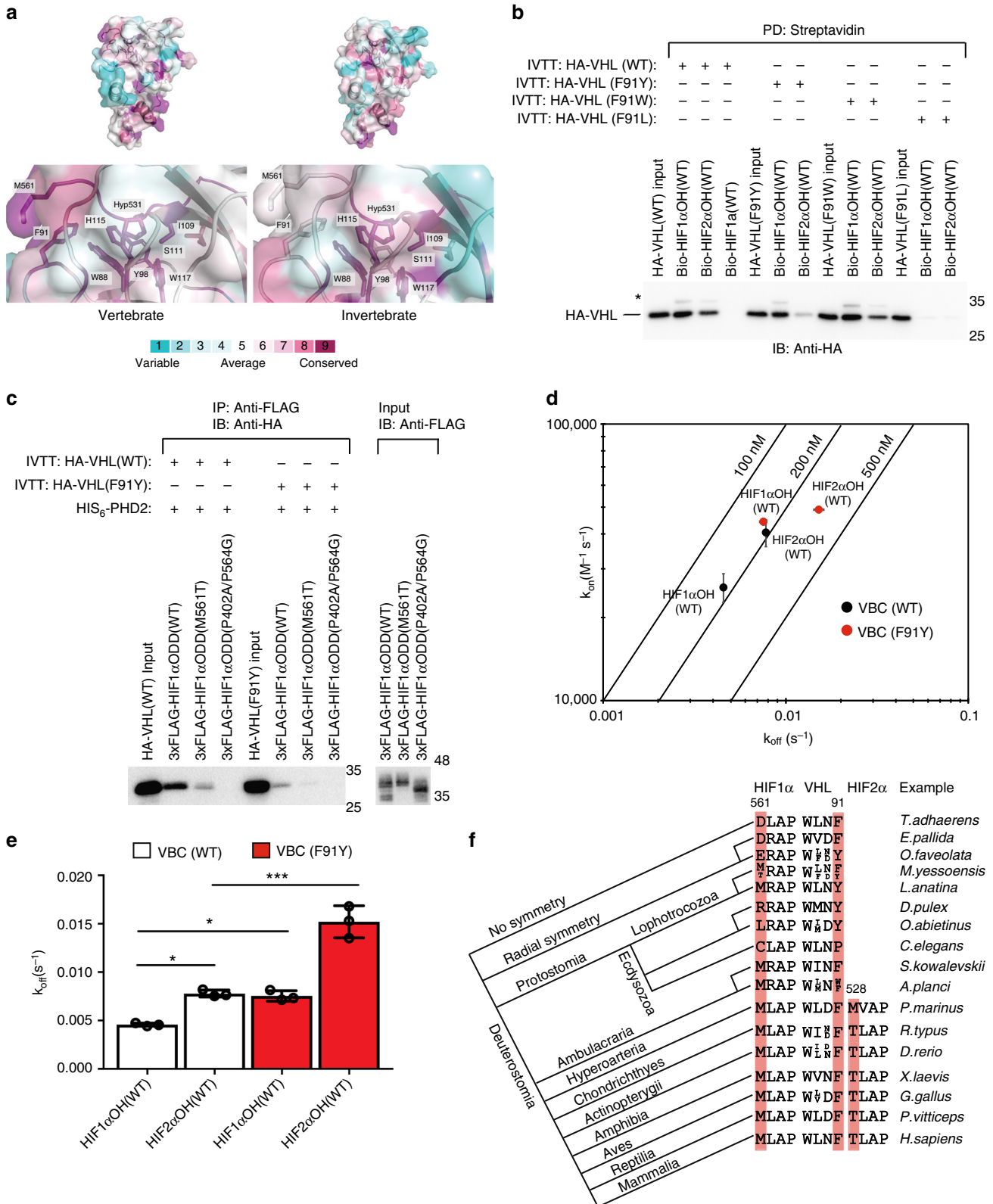


Fig. 4 Oxidation of HIF α Met $_{n-3}$ weakens the interaction between VHL and HIF α . **a** Structure of VHL-HIF2 α (6BVB) and VHL-HIF1 α (1LM8) were accessed from PDB and superimposed using Pymol. The distance and angle between HIF1 α Met561 (sulfur) and VHL Phe91 (center of aromatic ring) are indicated. **b, c** Biotinylated HIF α OH peptides were immobilized on streptavidin- agarose beads and incubated with in vitro transcribed and translated (IVTT) HA-VHL. Streptavidin beads were pulled down (PD) and levels of HA-VHL were visualized via immunoblotting (IB). **b** The solvent used to re-constitute the peptide is indicated. Molecular weight markers (kDa) are labeled for western blots. **d, e** Biolayer interferometry kinetic analysis of VHL-elongin B-elongin C (VBC) complex binding to immobilized HIF α peptides. Biotinylated peptides were immobilized on streptavidin- coated biosensors and binding to VBC complex was monitored. The data was analyzed assuming a 1:1 binding model via the BLITZ Pro software. **d** Rate plane with Isoaffinity Diagonals (RaPID) plot highlighting the kinetic parameters of VBC complex binding to HIF α peptides. Values represent mean of three experiments conducted with independently purified protein \pm s.e.m. **e** The dissociation constants associated with VBC binding to HIF α peptides are shown on a linear scale. Statistical significance was assessed using a one-way ANOVA with Tukey's post hoc test. Values represent mean of three experiments conducted with independently purified protein \pm s.d. * $p < 0.05$, *** $p < 0.005$

vertebrate species but variable among invertebrate species (Supplementary Fig. 3, 4a). Among the studied invertebrate species, nearly all possessed an aromatic residue, with VHL Tyr $_{n+3}$ being the most prevalent (Supplementary Fig. 4a). Only *C. elegans* possesses a non-aromatic residue, instead featuring a bulky proline residue (Supplementary Fig. 3). Employing the ConSurf server, HIF1 α and VHL amino acid residues were colour-coded in accordance to degree of conservation among the vertebrate and invertebrate lineage (Fig. 5a). Residues that form the hydroxylproline binding pocket, including VHL Trp88, VHL Tyr98, VHL Ile109, VHL Ser111, VHL His115, and VHL Trp117, are almost invariably conserved in both vertebrate and invertebrate species. Conversely, HIF1 α Met $_{n-3}$ and VHL Phe $_{n+3}$, which are adjacent to the hydroxylproline binding pocket, are variable in the invertebrate lineage (Fig. 5a).

Due to the intense negative selection that VHL Phe $_{n+3}$ is under in the vertebrate lineage, we next explored the pattern of HIF1 α and HIF2 α binding among VHL proteins with Phe91 substitutions. VHL F91W bound similarly to HIF1 α OH and HIF2 α OH peptides, when compared to VHL WT (Fig. 5b). Interestingly, VHL F91Y appeared to retain affinity for HIF1 α OH peptide but bound less HIF2 α OH peptide than VHL WT (Fig. 5b).

A F91L VHL mutation, which has been reported to cause VHL disease and sporadic RCC^{30,31}, was found to abolish binding to both HIF1 α or HIF2 α , suggesting that an aromatic residue in the $n + 3$ position is important for protein folding and/or stability. Further, we observed that VHL F91Y bound less HIF1 α ODD WT and HIF1 α ODD M561T than VHL WT, suggesting that VHL F91Y binds more weakly to HIF α independent of HIF α sequence determinants (Fig. 5c). The failure to observe decreased binding of VHL F91Y to HIF1 α WT in an in vitro pull-down assay may be due to saturation (Fig. 5b). Consistent with this notion, we observed that when less HIF1 α OH peptide was loaded on streptavidin agarose beads, the weaker affinity of HIF1 α OH peptide to VHL F91Y, compared with VHL WT, was readily observed (Supplementary Fig. 5). To further quantify the effect of the F91Y substitution on VHL/HIF α complex stability, we purified recombinant VHL F91Y (Supplementary Fig. 6). Using BLI, we confirmed that the F91Y substitution increases the dissociation rate of HIF1 α OH and HIF2 α OH peptide from VHL by roughly two-fold (Fig. 5d, e). Importantly, these results suggest that during the evolution of metazoans, particularly in the invertebrate lineage, substitution of VHL X $_{n+3}$ can modulate VHL/HIF α complex stability independently of HIF α sequence determinants.



Evolutionary fine-tuning of the HIF/VHL axis. Having observed that HIFα Met_{n-3} and VHL Phe_{n+3} residues result in a more stable HIFα/VHL complex, we next asked when these motifs emerged during invertebrate evolution. First, we inferred ancestral HIF1α sequences using a maximum parsimony method (Supplementary Fig. 7). The analysis suggests that the last

common ancestor of radiata and bilateria possessed a HIFα featuring Glu_{n-3} or Asp_{n-3}. However, the last common ancestor of deuterostome and protostome species is predicted to have featured HIFα Met_{n-3}. Among sampled protostome species, HIFα Met_{n-3} is observed most commonly in lophotrochozoa while substitutions are frequently observed in ecdysozoa species. All

Fig. 5 VHL Phe_{n+3} is associated with a more stable VHL/HIF α complex. **a** The structure of HIF1 α -VHL complex (PDB: 1LM8) is rendered as a cartoon superimposed with a transparent surface representation. Using multiple sequence alignments for VHL and HIF α in vertebrate and invertebrate species, amino acid residues were color-coded according to conservation using the ConSurf webserver. **b** Biotinylated HIF α OH peptides were immobilized on streptavidin- agarose beads and incubated with *in vitro* transcribed and translated (IVTT) HA-VHL. Streptavidin beads were pulled down (PD) and levels of HA-VHL were visualized via immunoblotting (IB). **c** 3xFLAG-HIF α oxygen-dependent degradation (ODD) domains were IVTT and incubated with purified HIS₆-PHD2 (181–426). Following hydroxylation (one hour), 3xFLAG-HIF α ODD domain was immobilized on protein A beads coated with anti-FLAG antibody and incubated with IVTT HA-VHL. 3xFLAG-HIF α ODD domain was immunoprecipitated (IP) and levels of HA-tagged VHL were visualized via immunoblotting (IB). Molecular weight markers (kDa) are labeled for western blots. **d, e** Biolayer interferometry kinetic analysis of VHL-elongin B-elongin C (VBC) complex binding to immobilized HIF α peptides. Biotinylated peptides were immobilized on streptavidin- coated biosensors and binding to VBC complex was monitored. The data was analyzed assuming a 1:1 binding model via the BLItz Pro software. **d** Rate plane with Isoaffinity Diagonals (RaPID) plot highlighting the kinetic parameters of VBC complex, either WT or F91Y, binding to HIF α peptides. Values represent mean of three experiments conducted with independently purified protein \pm s.e.m. **e** The dissociation constants associated with VBC binding to HIF α peptides are shown on a linear scale. Statistical significance was assessed using a one-way ANOVA with Tukey's post hoc test. Values represent mean of three experiments conducted with independently purified protein \pm s.d. * $p < 0.05$, *** $p < 0.005$. **f** An idealized phylogenetic tree of metazoan evolution is depicted. Short HIF1 α , HIF2 α , and VHL sequences from representative species are given

chordata species sampled featured HIF α Met_{n-3}. We attempted a similar analysis with VHL sequences, but generation of a phylogenetic tree that accurately separated species into known clades proved difficult. Manual inspection of VHL sequences revealed that non-bilaterian species may possess either VHL Phe_{n+3} or Tyr_{n+3}. Among protostome species, half of the examined lophotrochozoa possess VHL Phe_{n+3}, while all ecdysozoa species examined possess VHL Tyr_{n+3}. We next explored how often the VHL Phe_{n+3} and HIF α Met_{n-3} motifs co-exist in invertebrate species. As discussed, these residues are conserved in the vertebrate lineage. In the invertebrate lineage, more than half of all species (4/6) that contain HIF1 α Met_{n-3} possess a corresponding VHL Phe_{n+3} residue (Supplementary Fig. 4b). Conversely, species with VHL Tyr_{n+3} almost exclusively possess HIF α non-Met_{n-3} (7/8). The particular residue varies depending on the clade; Leu in order hymenoptera (*T. cornetzi*, *O. abietinus*), Glu in order scleractinia (*O. faveolata*, *S. pistillata*), Arg in genus daphnia (*D. pulex*, *D. magna*; Supplementary Fig. 3). Additionally, *M. yessoensis* (scallop) features both VHL Tyr_{n+3} and HIF α Thr_{n-3}, which co-immunoprecipitation and BLI studies revealed was the least stable HIF α -VHL complex, while other members of the family Ostreidae (*C. virginica*, *C. gigas*) possess both VHL Phe_{n+3} and HIF1 α Met_{n-3}, the most stable HIF α -VHL complex (Fig. 5c–e). These observations suggested that even within a group of closely related species, HIF α -VHL complex stability is variable and can potentially drive adaptation to their unique environments. Further, these observations led us to ask whether the combination of VHL Phe_{n+3} and HIF1 α Met_{n-3} emerged once during evolution or along multiple lineages. To tackle this question, we constructed an idealized phylogeny on the basis of well-characterized branching points during metazoan evolution (radial symmetry versus bilateral symmetry, protostome versus deuterostome; Fig. 5f). Among ecdysozoa species for which we have VHL and HIF α sequence data, none possess the combination of HIF α Met_{n-3} and VHL Phe_{n+3}. Among sampled lophotrochozoa, 2 out of 4 possess the combination of HIF α Met_{n-3} and VHL Phe_{n+3}. With the ubiquity of the HIF α Met_{n-3}/VHL Phe_{n+3} combination in deuterostomes and its absence in non-bilaterians, it becomes unclear whether species belonging to the ecdysozoa monophyletic clade experienced a loss of the HIF α Met_{n-3}/VHL Phe_{n+3} combination or whether the presence of this combination in species belong to the lophotrochozoa clade represents independent, convergent evolution. Considering our ancestral sequence analysis, which suggested that HIF α Met_{n-3} was present in the last common ancestor to lophotrochozoa and ecdysozoa species, a secondary loss in ecdysozoa seems more likely. However, a comprehensive phylogenetic study would need to be conducted in order to test this hypothesis. What is clear is that

among radiata and protostome species significant variation can be tolerated at the HIF α X_{n-3} and VHL Phe_{n+3} residues, while intense selective pressure seems to maintain HIF α Met_{n-3} and VHL Phe_{n+3} within the deuterostome clade.

In lamprey (*P. marinus*), a jawless, primitive vertebrate, both HIF1 α and HIF2 α feature Met_{n-3} (Fig. 5f). This finding suggests that the ancestral HIF α that duplicated during the evolution of vertebrates possessed Met_{n-3} and that Thr_{n-3} emerged following divergence of the evolutionary lineage that led to modern-day lampreys, which occurred approximately 500 million years ago³². Although we are greatly interested in the evolutionary underpinning of HIF1 α and HIF2 α regulation in mammals, further studies would be required to elucidate the relative stabilities of ancestral HIF α /VHL complexes. Such studies may reveal insight into the adaptation of the oxygen/hypoxia-sensing pathway to various environmental conditions (e.g., terrestrial versus aquatic environments). Our evaluation of HIF1 α M561A and NLE-substituted HIF1 α suggests that substitution of Met_{n-3} with less bulky amino acids would result in decreased complex stability. Further, we show that substitution of VHL Phe_{n+3} with Tyr decreases HIF α /VHL complex stability irrespective of the HIF α X_{n-3}. Thus, substitution of these interacting residues may allow for a fine-tuning of the hypoxia response pathway via modulation of HIF α /VHL complex stability without abrogating VHL-mediated regulation of HIF α entirely.

Discussion

Interaction of HIF α and VHL absolutely requires the hydroxylation of a conserved HIF α proline residue, which is hydrogen bonded to VHL residues and buried in a highly complementary pocket lined by bulky nonpolar residues. Here, we identify additional HIF α and VHL residues of evolutionary significance that can further stabilize the HIF α /VHL complex. The residues that line the hydroxylproline binding pocket are conserved in all examined metazoan species, suggesting that the mode of VHL/HIF α binding is well-preserved among invertebrate and vertebrate species (Fig. 5a). However, adjacent residues (i.e. HIF α X_{n-3} and VHL X_{n+3}) can also interact and, depending on the biochemical properties of the residues substituted at those positions, can stabilize the VHL/HIF α complex to varying degrees. Among radiata, we predict, on the basis of sequence alignments (Supplementary Fig. 3), that VHL Tyr_{n+3} is most prevalent and contacts a variable, non-Met residue on HIF α (Fig. 5f). Within the protostome clade, the combination of HIF α Met_{n-3}/VHL Phe_{n+3} is observed in half of the sampled lophotrochozoa species but never in sampled ecdysozoa species (Fig. 5f). Conversely, among deuterostome species we instead observe that VHL Phe_{n+3} and HIF α Met_{n-3} are conserved (Fig. 5f). Our biochemical and

biophysical experiments would suggest that HIF α /VHL complex stability is increased in deuterostome invertebrates, from which vertebrate species evolved, compared to radiata and protostome species (Fig. 5c–e).

Two other evolutionary trends in hypoxia-sensing have been noted in invertebrate species. First, it has been well-described that HIF α in non-bilateria species only have one ODD site while most protostome and deuterostome species feature two ODD sites. Second, while the *T. adhaerens* genome only encodes one PHD protein (most similar to human PHD2), invertebrate eumetazoan genomes, with the exception of protostomes, contain two PHD genes⁷. These two evolutionary trends have intersected. For example, human PHD3 specifically hydroxylates HIF1 α CODD but not NODD³³. Both of these evolutionary events (ODD and PHD duplication) appeared in the metazoan lineage before the HIF α Met_{n-3}/VHL Phe_{n+3} secondary contact site became fixed. The evolution of a secondary ODD site and duplication of an ancestral PHD gene allows for a more fine-tuned, and possibly stronger, negative regulation.

Upon the evolution of vertebrate species, the ancestral HIF α gene went through several rounds of duplication, yielding multiple related transcription factors, with HIF1 α and HIF2 α thought to be the most important. Interestingly, an incredibly conserved substitution of HIF1 α Met_{n-3} to HIF2 α Thr_{n-3} occurred sometime after lamprey diverged from other vertebrate species (Fig. 5f). This substitution has been demonstrated to decrease the affinity of HIF2 α for VHL by roughly two to three-fold when biochemical experiments are conducted with peptides and proteins corresponding to the human sequences (Fig. 1, Fig. 2, Supplementary Fig. 1, Supplementary Fig. 2). Thus, two important transitions need to be discussed; the transition from what is predicted to be a weaker HIF1 α /VHL complex in some radiata and protostome species to a stronger complex in deuterostomes and the divergence of HIF1 α and HIF2 α , with respect to affinity for VHL, in the vertebrate lineage.

Animals first diversified between 600 and 500 million years ago under conditions that today would be described as hypoxic. One emergent model of hypoxia sensing and metazoan evolution focuses on the propensity for oxic niches to promote cell differentiation³⁴. For example, primary non-malignant breast tissue can be maintained in an immature state when grown under hypoxic conditions, whereas normoxic conditions promote terminal differentiation³⁵. An established body of work shows that hypoxia promotes survival of primitive hematopoietic stem cells^{36–39}. Furthermore, activation of HIF2 α is associated with sympathetic nervous system tumours with particular importance in the cancer stem cell population^{40–42}. With these observations in mind, it has been suggested that the ability of HIF2 α to promote a pseudohypoxic state conducive to self-renewal and proliferative properties in adult stem cell populations was evolutionarily advantageous³⁴. By extension, rather than HIF α evolving as a mechanism to allow cells to survive low oxygen states, HIF α might have been necessary for the maintenance of stem cell populations under high oxygen conditions. The observation that HIF2 α is stabilized under higher oxygen tensions (up to 7% O₂) than HIF1 α (~2% O₂) suggests that, upon duplication of ancestral HIF α , the two paralogs specialized with HIF2 α assuming the role of pseudohypoxia maintenance in select cell types³⁴. However, in invertebrate species possessing only a single HIF α gene, a balance would need to be struck between the ability to maintain a pseudohypoxic niche and inducibility under oxygen tensions that impede on an organism's preferred metabolism. One can imagine that if pseudohypoxic maintenance was the only concern, an 'ideal' HIF α would lack an ODD domain entirely. We will now directly discuss our presented results with emphasis on this 'pseudohypoxic' model. We speculate that the relative rarity

of the HIF α Met_{n-3}/VHL Phe_{n+3} motif in radiata and protostome species may represent an evolutionary pressure towards stabilization of HIF α at higher oxygen tensions (i.e. less efficient degradation). In this model, ancestral HIF α would be more stable and promote a pseudohypoxic state that is critical for stem cell niches yet could be further induced under hypoxia. Conversely, invertebrate deuterostome species possess HIF1 α Met_{n-3} and VHL Phe_{n+3}. In these species, other means of maintaining a pseudohypoxic niche may augment the HIF-mediated strategy. Generally speaking, the increased variability in HIF1 α and VHL sequences among invertebrate species, particularly among the residues that we have studied, may reflect a fine-tuning of pseudohypoxic maintenance and metabolic regulation under hypoxic insult (Fig. 3b). If pseudohypoxic maintenance is an important HIF α role in invertebrate species, we would expect that HIF α protein should be present at detectable levels under ambient atmospheric conditions, much like HIF2 α in mammalian cells.

One limitation of our interpretation of invertebrate HIF evolution is that we studied 'ancestral' HIF and VHL substitutions in the context of otherwise human protein and peptide sequences. Studies with full-length VHL and HIF α proteins from representative invertebrate species would be required to further speculate on the evolution of oxygen-sensitivity in HIF α proteins. For example, although radiata and protostome species rarely feature HIF α Met_{n-3}, HIF α Arg_{n-3} and Arg/Lys_{n-2} are frequently observed. Interestingly, Arg/Lys can participate in stable cation- π interactions with aromatic residues, which may functionally compensate for absence of HIF α Met_{n-3}⁴³. As full-length HIF α proteins have been difficult to purify, another potential limitation of our study is the use of HIF α peptides as a surrogate for full-length or ODD recombinant protein. However, the peptide design we utilized is sufficient for VHL interaction, and the affinity of IVTT HIF α ODD protein for VHL can be modulated by substitution of amino acid X_{n-3} in a manner that mirrors our biophysical and biochemical peptide studies (Fig. 2f, Supplementary Fig. 1c). As our immunoprecipitation studies with HIF α ODD and VHL require prior hydroxylation of HIF α via recombinant PHD2, we have reason to believe that overall post-translational regulation of HIF1 α is weakened by the Thr_{n-3} substitution. However, it remains important to study how PHD-mediated regulation of HIF α has evolved in metazoans, paying close attention to the variable number of HIF α ODD sites and PHD proteins expressed in various invertebrate species.

Early vertebrate genome duplications also contributed to the diversification and specialization of HIF pathway as an expanded repertoire of hypoxia sensitive transcription factors allowed for functional specialization. Our biophysical study of HIF1 α and HIF2 α binding affinity for VHL suggests that substitutions of amino acid residues proximal to the primary hydroxylation site played a role in the divergence of HIF1 α and HIF2 α in the vertebrate lineage. Although research into the biochemistry of HIF α in invertebrate species is lacking, evolution of the HIF1 α coding sequence has been studied extensively in fish, including the family cyprinidae, which retained two copies of HIF1 α (HIF1 α A/B) and HIF2 α (HIF2 α A/B). In cyprinids, NODD is lost specifically in HIF1 α A^{44,45}. In vivaporous eelpout (*Zoarces viviparous*), which belongs to the family Zoarcidae, the NODD proline is substituted with a leucine residue⁴⁶. In teleost species, the NODD region is generally less conserved than the CODD region⁴⁶. Moreover, human HIF2 α NODD is poorly hydroxylated by PHD2, which can effectively hydroxylate HIF1 α NODD⁴⁷. These observations correlate well with the elevated rate of non-synonymous mutation in HIF2 α NODD in vertebrates, including both teleosts and mammals, when compared to either HIF2 α CODD or HIF1 α NODD²⁶. Generally, these substitutions appear to affect only one paralog, resulting in an increasingly fine-tuned hypoxia response

in vertebrate species, where one gene paralog is potentially stabilized over a wider range of oxygen tensions and may be of particular importance for pseudohypoxia maintenance.

Further work has been conducted to explore whether substitution of HIF α residues witnessed along an evolutionary branch can modulate HIF α stability. A more direct parallel to our observation is seen in Cyprinid fish belonging to the genus *Schizothorax*, which are well-adapted to hypoxic conditions present in the Tibetan plateau. These fish exhibit a substitution of HIF1 α B L_{n-5}, which is associated with increased stability of the protein⁴⁴. Other missense HIF2 α mutations have been observed to be enriched in high-altitude populations, including a Q579L mutation in Tibetan cashmere goat (*Capra hircus*)⁴⁸ and G305S in several species of high-altitude dog⁴⁹. However, the functional effects of these mutations, if any, have yet to be discerned. Overall, it is clear that substitutions in the coding sequence of HIF α allows for modulation of HIF α signalling activity, in part, by modulating negative regulation via PHD and/or VHL.

We observed that the VHL F91Y substitution, which is invariant in vertebrate species, resulted in lower affinity for both HIF2 α and HIF1 α (Fig. 5c–f). The intense purifying selection that maintains VHL Phe_{n+3} in the vertebrate lineage may reflect a decrease in fitness associated with excessive stabilisation of HIF2 α . Concordantly, HIF2 α -activating mutations in humans have been associated with either polycythemia, a condition of elevated hematocrit, or neuroendocrine tumours, including paraganglioma, pheochromocytoma, and somatostatinoma^{41,50}. We previously identified disease-causing mutations of residues proximal to the CODD hydroxylation site that result in only mild stabilisation of the HIF2 α protein¹². Thus, further stabilisation of HIF2 α can be deleterious at the organismal level.

Although the strong conservation of HIF α Met_{n-3} in the vertebrate lineage does support our hypothesis that divergence of HIF1 α and HIF2 α affinity for VHL is of biological importance, our VHL/HIF α binding experiments also suggest that the insertion of HIF2 α Gly_{n+6} does not overtly modulate complex stability (Fig. 2b, d). Thus, it appears that conservation of a residue proximal to HIF α hydroxylation sites does not necessarily suggest that the residue is of importance but instead may reflect fixation of a substitution that is (nearly) neutral. However, a second possibility is that HIF2 α Gly_{n+6} modulates regulation via PHD enzymes. It has been previously shown that modulation of the distance between HIF1 α P564 and HIF1 α L574, by insertion or deletion of aspartate residues, increases PHD-mediated hydroxylation⁵¹. Thus, it is possible that an insertion of glycine alters the interaction of HIF2 α with PHDs.

In conclusion, we reveal that HIF α /VHL complex stability is modulated by substitutions in HIF α and VHL residues that are relevant to metazoan evolution. Notably, human HIF1 α and HIF2 α proteins intrinsically differ in their affinity for VHL and that the underlying molecular evolution suggests that specialization of HIF1 α and HIF2 α in the vertebrate lineage has been maintained by intense purifying selection. Future work on the molecular evolution of HIF α and VHL may reveal further insight into the unique roles of HIF1 α and HIF2 α in human biology and the dual roles of metabolic regulation and pseudohypoxic maintenance in early metazoan evolution.

Methods

Plasmids. Construction of the following plasmids has been described previously; pcDNA3-HA-VHL₃₀, pcDNA3-HA-HIF1 α ³, pACYCDuet-1 plasmid encoding untagged elongin B and elongin C(17–112), pGEX-4T-1-GST-VHL₁₉(54–213)⁵², pcDNA3-3xFLAG-HIF2 α ODD(390–554; both WT and P531A), and pET-46-HIS₆-PHD2¹². F91Y, F91L, and F91W mutations were introduced into the pcDNA3-HA-VHL₃₀ and pGEX-4T-1-GST-VHL₁₉ plasmids via site-directed mutagenesis. pcDNA3-3xFLAG-HIF2 α ODD P405A/P531A double-mutant was generated via site-directed mutagenesis of pcDNA3-3xFLAG-HIF2 α ODD P531A.

pcDNA3-3xFLAG-HIF1 α ODD (387–581) was sub-cloned from full-length pcDNA3-HA-HIF1 α . The pcDNA3-3xFLAG-HIF1 α ODD (387–581; P402A/P564G double-mutant) was sub-cloned from a full-length HIF1 α P402A/P564G construct generously gifted by from Dr. Norma Masson and the lab of Dr. Peter Ratcliffe. HIF2 α T528M and HIF1 α M561T constructs were generated in both the ODD and full-length HIF α vectors. All primers used for cloning are listed in Supplementary Table 1.

Antibodies. Anti-HA (C29F4; 1:2000 dilution western blot) was obtained from Cell Signaling Technology. Anti-FLAG (F1804; 1:5000 dilution western blot; 1:1000 dilution immunoprecipitation) was obtained from Sigma-Aldrich.

Peptides. HIF- α peptides, with N-terminal biotinylation and C-terminal amidation modifications, were custom synthesized by Genscript. For pVHL interaction studies, WT HIF1 α (556–573; DLDLEMLA[*Hyp*]YIPMDDDDFQ) and WT HIF2 α (523–541; ELDLETLA[*Hyp*]YIPMDGEDFQ) were used, where *Hyp* denotes hydroxyproline. Peptides were reconstituted to 2 mg/mL, as measured by A280, using either sterile DMSO or 0.1 M ammonium bicarbonate pH 9.0 buffer. Peptides were aliquoted and stored at –80 °C.

In vitro binding assay. The in vitro pVHL-HIF α binding assay was performed as previously described⁵². HA-VHL₃₀ was expressed in an IVTT rabbit reticulocyte lysate system (Promega, Cat. No. L1170) and incubated with 1.2 μ g of biotinylated HIF α OH peptide immobilized on streptavidin agarose beads in 500 μ L of EBC buffer (50 mM Tris-HCl pH 8.0, 120 mM NaCl, 0.5% (v/v) NP-40) for two hours at 4 °C. To perform a competition binding assay, 1.8 μ g of biotinylated HIF α OH peptide immobilized on streptavidin agarose beads competed with 1 μ g of acetylated HIF α OH peptide. Following incubation, beads were washed 4x with NETN buffer (20 mM Tris-HCl pH 8.0, 100 mM NaCl, 1 mM EDTA, 0.5% (v/v) NP-40). Biotinylated peptide was pulled down via streptavidin agarose beads and protein was eluted by boiling beads in sample buffer. Protein levels of HA-VHL₃₀ were determined by immunoblotting.

Biolayer interferometry. The binding affinities of VBC to hydroxylated HIF α peptide was measured by biolayer interferometry using the BLItz system (Pall ForteBio). A 50 μ g/mL solution of biotinylated HIF α peptide was prepared in kinetics buffer (20 mM HEPES pH 7.4, 200 mM NaCl, 1 mM DTT, 0.02% (v/v) Tween-20, and 0.5% (w/v) BSA) and immobilized onto streptavidin (SA)-coated biolayer interferometry (BLI) biosensors (Pall ForteBio, Cat. No. 18–5019) over 120 s. Multiple concentrations of purified VBC complex were diluted in kinetics buffer and allowed to associate with immobilized peptide over 120 s. Subsequently, the SA-BLI probe was immersed into kinetics buffer for 120 s to allow for dissociation. Both protein and buffer were chilled on ice immediately before use. The data were analyzed, step corrected, reference corrected, and fit to a global 1:1 binding model. K_d , k_a , and k_d were calculated using the BLItz Pro software. All measurements were performed in triplicate with independently purified recombinant protein.

Surface plasmon resonance. Single cycle kinetics experiments were conducted with the Biacore X100 (GE Healthcare Life Sciences, Cat. No. BR110073) at 25 °C. A 125 ng/mL solution of HIF α peptide was prepared in running buffer (20 mM HEPES pH 7.4, 200 mM NaCl, 0.02% (v/v) Tween-20, 1 mg/mL BSA) and immobilized using a biotin CAPture kit (GE Healthcare Life Sciences, Cat. No. 28920233) over 120 s. VBC was serially diluted in running buffer (0.123 μ g/mL, 0.37 μ g/mL, 1.11 μ g/mL, 3.33 μ g/mL, 10 μ g/mL) and flowed over the SPR chip for 120 s at a flow rate of 30 μ L/min, with a final dissociation step of 600 s. The data was double-referenced and fit to a global 1:1 binding model.

In vitro hydroxylation assay. 3xFLAG-HIF α ODD was expressed via the rabbit reticulocyte lysate system. HIF α ODD was incubated with 15 μ g/ μ L HIS₆-PHD2 (181–426) in 200 μ L of 40 mM HEPES pH 7.4, 80 mM KCl, 5 mM α -ketoglutarate, 2 mM ascorbic acid, 100 μ M FeCl₂ tetrahydrate solution at 30 °C for 1 h. Following hydroxylation, 3xFLAG-HIF α was incubated with IVTT VHL₃₀ in 500 μ L of wash buffer (40 mM HEPES pH 7.4, 80 mM KCl, 0.05% (v/v) Tween-20, 250 μ M EDTA, 1 mM DTT) supplemented with protease inhibitors for 2 h at 4 °C. Following binding, 3xFLAG-HIF α ODD was immunoprecipitated with anti-FLAG antibody immobilized on protein A beads. Protein was eluted by boiling beads in sample buffer. Protein levels of HA-VHL₃₀ were determined by immunoblotting.

Structural analysis. Structures of VHL-HIF1 α OH complex (1LM8, 1LQB)^{10,11} and VHL-HIF2 α OH complex (6BVB)¹² were accessed via PDB. Structures were superimposed using Pymol. Proteins, Interfaces, Structures, and Assemblies was used to evaluate the structural interface of HIF α /VHL.

Alignment. Annotated HIF1 α , HIF2 α , and VHL sequences were identified with the BLASTP algorithm accessed with the Mega7 software⁵³. Sequence identifiers are listed in Supplementary Table 2. Full-length amino acid sequences were aligned

using the GUIDANCE2 webserver via the MAFFT algorithm with 100 bootstrap repeats and 1000 cycles of iterative refinement⁵⁴. Full-length HIF1 α cDNA sequences were aligned as codons using the GUIDANCE2 webserver as described above. Nematode sequences were not included for multiple sequence alignment (MSA) of cDNA as they were unreliably aligned according to confidence scores generated by GUIDANCE2. The ODD domain was defined as the sequence that aligned with human HIF1 α codons 359–598. ODD sequences were re-aligned as described above. A SuperMSA was created by concatenating the top alignment with 20 alternative alignments. The SuperMSA contained 10435 codons, including gaps. Alignments were visualized using ESPript⁵⁵.

Phylogenetic analysis. The SuperMSA was used to generate a reference phylogenetic tree. Smart Model Selection (SMS) was accessed via the PhyML 3.0 webserver to select a model for generating a maximum-likelihood phylogenetic tree⁵⁶. A phylogenetic tree was constructed with a generalized time reversible (GTR) substitution model with four substitution rate categories (gamma factor of 1.374) and a fraction of sites allowed to be invariant (0.015)⁵⁷. Branch support was determined by performing 100 bootstraps. *T. adhaerens* was selected as the outgroup. FigTree was used to visualize phylogenetic trees (<http://tree.bio.ed.ac.uk/software/figtree/>).

Estimating selective pressure. The HyPhy package, accessed via Mega7 software, was used to estimate synonymous and non-synonymous mutation rates for codons among vertebrates and invertebrate species based on the top MSA generated via GUIDANCE2. The above-described maximum-likelihood phylogenetic tree was used as reference. The GTR substitution model was used and all columns containing gaps were deleted.

Consurf was used to generate visual representations of HIF1 α and VHL evolutionary conservation at the amino acid level⁵⁸. The co-structure of HIF1 α peptide bound to VHL was accessed from PDB (1LM8). Separate amino acid alignment of VHL and HIF1 α were provided for vertebrate and invertebrate species. The *H. sapien* sequence was included for the invertebrate alignment to accurately project alignment information onto the structure of human VHL bound to HIF1 α .

Inferring ancestral sequence. Using Mega7 software, ancestral amino acid states were inferred using the Maximum Parsimony method. The set of states at each node is ordered from most likely to least likely, excluding states with probabilities below 5%. The above-described maximum-likelihood phylogenetic tree was used as reference.

Quantification and statistical analysis. To evaluate statistical significance of dissociation constants, a one-way ANOVA with Tukey post hoc test was conducted using Prism software. A *p* value below 0.05 was considered significant.

Reporting summary. Further information on research design is available in the Nature Research Reporting Summary linked to this article.

Data availability

Source data for Figs. 1a, 1b, 2b, 2c, 2d, 2e, 3a, 3b, 3c, 4b, 4c, 4d, 4e, 5b, 5c, 5d, 5e, and supplementary Figs. 1a, 1b, 1c, 2a, 2b, 2c, 4a, 4b, 5, 6b are provided as a Source Data file. All data are available from the corresponding author upon reasonable request.

Received: 31 January 2019 Accepted: 26 June 2019

Published online: 23 July 2019

References

- Kaelin, W. G. Jr. & Ratcliffe, P. J. Oxygen sensing by metazoans: the central role of the HIF hydroxylase pathway. *Mol. Cell* **30**, 393–402 (2008).
- Epstein, A. C. et al. *C. elegans* EGL-9 and mammalian homologs define a family of dioxygenases that regulate HIF by prolyl hydroxylation. *Cell* **107**, 43–54 (2001).
- Ohh, M. et al. Ubiquitination of hypoxia-inducible factor requires direct binding to the beta-domain of the von Hippel-Lindau protein. *Nat. Cell Biol.* **2**, 423–427 (2000).
- Maxwell, P. H. et al. The tumour suppressor protein VHL targets hypoxia-inducible factors for oxygen-dependent proteolysis. *Nature* **399**, 271–275 (1999).
- Jaakkola, P. et al. Targeting of HIF- α to the von Hippel-Lindau ubiquitylation complex by O₂-regulated prolyl hydroxylation. *Science* **292**, 468–472 (2001).
- Mills, D. B. et al. The last common ancestor of animals lacked the HIF pathway and respired in low-oxygen environments. *Elife* **7**, e31176 (2018).
- Loenarz, C. et al. The hypoxia-inducible transcription factor pathway regulates oxygen sensing in the simplest animal, *Trichoplax adhaerens*. *EMBO Rep.* **12**, 63–70 (2011).
- Lippel, K. et al. Born to sense: biophysical analyses of the oxygen sensing prolyl hydroxylase from the simplest animal *Trichoplax adhaerens*. *Hypoxia* **6**, 57 (2018).
- Lendahl, U., Lee, K. L., Yang, H. & Poellinger, L. Generating specificity and diversity in the transcriptional response to hypoxia. *Nat. Rev. Genet.* **10**, 821 (2009).
- Hon, W. C. et al. Structural basis for the recognition of hydroxyproline in HIF-1 α by pVHL. *Nature* **417**, 975–978 (2002).
- Min, J. H. et al. Structure of an HIF-1 α –pVHL complex: hydroxyproline recognition in signaling. *Science* **296**, 1886–1889 (2002).
- Tarade D., Robinson C. M., Lee J. E., Ohh M. HIF-2 α -pVHL complex reveals broad genotype-phenotype correlations in HIF-2 α -driven disease. *Nat. Commun.* **9**, 3359 (2018).
- Wu, D., Potluri, N., Lu, J., Kim, Y. & Rastinejad, F. Structural integration in hypoxia-inducible factors. *Nature* **524**, 303 (2015).
- Ryan, H. E., Lo, J. & Johnson, R. S. HIF-1 α is required for solid tumor formation and embryonic vascularization. *EMBO J.* **17**, 3005–3015 (1998).
- Iyer, N. V. et al. Cellular and developmental control of O₂ homeostasis by hypoxia-inducible factor 1 α . *Genes Dev.* **12**, 149–162 (1998).
- Peng, J., Zhang, L., Drysdale, L. & Fong, G.-H. The transcription factor EPAS-1/hypoxia-inducible factor 2 α plays an important role in vascular remodeling. *Proc. Natl Acad. Sci. USA* **97**, 8386–8391 (2000).
- Tian, H., Hammer, R. E., Matsumoto, A. M., Russell, D. W. & McKnight, S. L. The hypoxia-responsive transcription factor EPAS1 is essential for catecholamine homeostasis and protection against heart failure during embryonic development. *Genes Dev.* **12**, 3320–3324 (1998).
- Schodel, J. et al. High-resolution genome-wide mapping of HIF-binding sites by ChIP-seq. *Blood* **117**, e207–e217 (2011).
- Smythies, J. A. et al. Inherent DNA-binding specificities of the HIF-1 α and HIF-2 α transcription factors in chromatin. *EMBO Rep.* **20**, e46401 (2019).
- Fu, L., Wang, G., Shevchuk, M. M., Nanus, D. M. & Gudas, L. J. Generation of a mouse model of Von Hippel-Lindau kidney disease leading to renal cancers by expression of a constitutively active mutant of HIF1 α . *Cancer Res.* **71**, 6848–6856 (2011).
- Schönenberger, D. et al. Formation of renal cysts and tumors in Vhl/Trp53-deficient mice requires HIF1 α and HIF2 α . *Cancer Res.* **76**, 2025–2036 (2016).
- Fu, L., Wang, G., Shevchuk, M. M., Nanus, D. M. & Gudas, L. J. Activation of HIF2 α in kidney proximal tubule cells causes abnormal glycogen deposition but not tumorigenesis. *Cancer Res.* **73**, 2916–2925 (2013).
- Kondo, K., Kim, W. Y., Lechpammer, M. & Kaelin, W. G. Jr. Inhibition of HIF2 α is sufficient to suppress pVHL-defective tumor growth. *PLoS Biol.* **1**, E83 (2003).
- Zimmer, M., Doucette, D., Siddiqui, N. & Iliopoulos, O. Inhibition of hypoxia-inducible factor is sufficient for growth suppression of VHL-/- tumors1 1 NIH grant R29CA78358-06 (OI), Bertucci Fund for Urologic Malignancies (OI), David P. Foss Fund (OI), and VHL Family Alliance 2003 award (MZ). *Mol. Cancer Res.* **2**, 89–95 (2004).
- Holmquist-Mengelbier, L. et al. Recruitment of HIF-1 α and HIF-2 α to common target genes is differentially regulated in neuroblastoma: HIF-2 α promotes an aggressive phenotype. *Cancer Cell* **10**, 413–423 (2006).
- Rytönen, K. T., Williams, T. A., Renshaw, G. M., Primmer, C. R. & Nikinmaa, M. Molecular evolution of the metazoan PHD–HIF oxygen-sensing system. *Mol. Biol. Evol.* **28**, 1913–1926 (2011).
- Valley, C. C. et al. The methionine-aromatic motif plays a unique role in stabilizing protein structure. *J. Biol. Chem.* **287**, 34979–34991 (2012).
- Lewis, A. K. et al. Oxidation increases the strength of the methionine-aromatic interaction. *Nat. Chem. Biol.* **12**, 860 (2016).
- Orabi, E. A. & English, A. M. Predicting structural and energetic changes in Met-aromatic motifs on methionine oxidation to the sulfoxide and sulfone. *Phys. Chem. Chem. Phys.* **20**, 23132–23141 (2018).
- Brauch, H. et al. VHL mutations in renal cell cancer: does occupational exposure to trichloroethylene make a difference? *Toxicol. Lett.* **151**, 301–310 (2004).
- Gallou, C. et al. Genotype-phenotype correlation in von Hippel-Lindau families with renal lesions. *Hum. Mutat.* **24**, 215–224 (2004).
- Smith, J. J. et al. Sequencing of the sea lamprey (*Petromyzon marinus*) genome provides insights into vertebrate evolution. *Nat. Genet.* **45**, 415 (2013).
- Chowdhury, R. et al. Structural basis for oxygen degradation domain selectivity of the HIF prolyl hydroxylases. *Nat. Commun.* **7**, 12673 (2016).
- Hammarlund E. U., Von Stedingk K., Pählman S. Refined control of cell stemness allowed animal evolution in the oxic realm. *Nat. Ecol. Evol.* **2**, 220–228 (2018).
- Vaapil, M. et al. Hypoxic conditions induce a cancer-like phenotype in human breast epithelial cells. *PLoS ONE* **7**, e46543 (2012).

36. Ivanović, Z., Sbarba, P. D., Trimoreau, F., Faucher, J. L. & Praloran, V. Primitive human HPCs are better maintained and expanded in vitro at 1 percent oxygen than at 20 percent. *Transfusion* **40**, 1482–1488 (2000).
37. Hermitte, F., de La Grange, P. B., Belloc, F., Praloran, V. & Ivanovic, Z. Very low O₂ concentration (0.1%) favors G0 return of dividing CD34+ cells. *Stem Cells* **24**, 65–73 (2006).
38. Rouault-Pierre, K. et al. HIF-2 α protects human hematopoietic stem/progenitors and acute myeloid leukemic cells from apoptosis induced by endoplasmic reticulum stress. *Cell Stem Cell* **13**, 549–563 (2013).
39. Mantel, C. R. et al. Enhancing hematopoietic stem cell transplantation efficacy by mitigating oxygen shock. *Cell* **161**, 1553–1565 (2015).
40. Pietras, A. et al. HIF-2 α maintains an undifferentiated state in neural crest-like human neuroblastoma tumor-initiating cells. *Proc. Natl Acad. Sci. USA* **106**, 16805–16810 (2009).
41. Zhuang, Z. et al. Somatic HIF2A gain-of-function mutations in paraganglioma with polycythemia. *N. Engl. J. Med* **367**, 922–930 (2012).
42. Li, Z. et al. Hypoxia-inducible factors regulate tumorigenic capacity of glioma stem cells. *Cancer Cell* **15**, 501–513 (2009).
43. Dougherty, D. A. Cation- π interactions involving aromatic amino acids. *J. Nutr.* **137**, 1504S–1508S (2007).
44. Guan, L., Chi, W., Xiao, W., Chen, L. & He, S. Analysis of hypoxia-inducible factor alpha polyploidization reveals adaptation to Tibetan plateau in the evolution of schizothoracine fish. *BMC Evol. Biol.* **14**, 192 (2014).
45. Rytönen, K. T. et al. Subfunctionalization of cyprinid hypoxia-inducible factors for roles in development and oxygen sensing. *Evolution* **67**, 873–882 (2013).
46. Rytönen, K. T., Vuori, K. A., Primmer, C. R. & Nikinmaa, M. Comparison of hypoxia-inducible factor-1 alpha in hypoxia-sensitive and hypoxia-tolerant fish species. *Comp. Biochem. Physiol. Part D: Genom. Proteom.* **2**, 177–186 (2007).
47. Appelhoff, R. J. et al. Differential function of the prolyl hydroxylases PHD1, PHD2, and PHD3 in the regulation of hypoxia-inducible factor. *J. Biol. Chem.* **279**, 38458–38465 (2004).
48. Song, S. et al. Exome sequencing reveals genetic differentiation due to high-altitude adaptation in the Tibetan cashmere goat (*Capra hircus*). *BMC Genom.* **17**, 122 (2016).
49. Gou, X. et al. Whole genome sequencing of six dog breeds from continuous altitudes reveals adaptation to high-altitude hypoxia. *Genome Res.* **171876**, 171113 (2014).
50. Percy, M. J. et al. Novel exon 12 mutations in the HIF2A gene associated with erythrocytosis. *Blood* **111**, 5400–5402 (2008).
51. Kageyama, Y. et al. Leu-574 of human HIF-1 α is a molecular determinant of prolyl hydroxylation. *FASEB J.* **18**, 1028–1030 (2004).
52. Heir, P. et al. Oxygen-dependent regulation of erythropoietin receptor turnover and signaling. *J. Biol. Chem.* **291**, 7357–7372 (2016).
53. Kumar, S., Stecher, G. & Tamura, K. MEGA7: molecular evolutionary genetics analysis version 7.0 for bigger datasets. *Mol. Biol. Evol.* **33**, 1870–1874 (2016).
54. Sela, I., Ashkenazy, H., Katoh, K. & Pupko, T. GUIDANCE2: accurate detection of unreliable alignment regions accounting for the uncertainty of multiple parameters. *Nucleic Acids Res.* **43**, W7–W14 (2015).
55. Robert, X. & Gouet, P. Deciphering key features in protein structures with the new ENDscript server. *Nucleic Acids Res.* **42**, W320–W324 (2014).
56. Lefort, V., Longueville, J.-E. & Gascuel, O. SMS: smart model selection in PhyML. *Mol. Biol. Evol.* **34**, 2422–2424 (2017).
57. Guindon, S. et al. New algorithms and methods to estimate maximum-likelihood phylogenies: assessing the performance of PhyML 3.0. *Syst. Biol.* **59**, 307–321 (2010).
58. Ashkenazy, H. et al. ConSurf 2016: an improved methodology to estimate and visualize evolutionary conservation in macromolecules. *Nucleic Acids Res.* **44**, W344–W350 (2016).

Acknowledgements

We thank the members of Ohh and Lee labs for their critical comments and discussions. We also thank Drs. Megha Shah, Trevor F. Moraes and James M. Rini for help with SPR experimentation and analysis. This work was supported by grants from the Canadian Institutes of Health Research (CIHR) (MOP-133694 to J.E.L.; PJT-159773 to M.O.). D.T. is a recipient of Vanier-CIHR Canada Graduate Scholarship.

Author contributions

M.O. and D.T. conceptualized the project and study design. D.T. performed all experiments. J.E.L. aided in designing, performing, and writing the biophysical experiments. D.T. and M.O. wrote the paper.

Additional information

Supplementary Information accompanies this paper at <https://doi.org/10.1038/s41467-019-11149-1>.

Competing interests: The authors declare no competing interests.

Reprints and permission information is available online at <http://npg.nature.com/reprintsandpermissions/>

Peer review information: *Nature Communications* thanks Alessio Ciulli and other anonymous reviewer(s) for their contribution to the peer review of this work. Peer reviewer reports are available.

Publisher's note: Springer Nature remains neutral with regard to jurisdictional claims in published maps and institutional affiliations.



Open Access This article is licensed under a Creative Commons Attribution 4.0 International License, which permits use, sharing, adaptation, distribution and reproduction in any medium or format, as long as you give appropriate credit to the original author(s) and the source, provide a link to the Creative Commons license, and indicate if changes were made. The images or other third party material in this article are included in the article's Creative Commons license, unless indicated otherwise in a credit line to the material. If material is not included in the article's Creative Commons license and your intended use is not permitted by statutory regulation or exceeds the permitted use, you will need to obtain permission directly from the copyright holder. To view a copy of this license, visit <http://creativecommons.org/licenses/by/4.0/>.

© The Author(s) 2019